Preprints of the 21st IFAC World Congress (Virtual)
Berlin, Germany, July 12-17, 2020

Command-Shaping Control of Linear Resonant Actuators for Haptic Force Generation

Franziska Schlagenhauf * **William Singhose** ** [1]
Khalid Sorensen *** [1] **Kelly Dobson** ****

* *Google LLC, Mountain View, CA 94043 USA (fschlagenhauf@google.com)*
** *Woodruff School of Mechanical Engineering, Georgia Institute of Technology, Atlanta, GA 30318 USA (Singhose@gatech.edu)*
*** *Woodruff School of Mechanical Engineering, Georgia Institute of Technology, Atlanta, GA 30318 USA (KhalidS@gatech.edu)*
**** *Google LLC, Mountain View, CA 94043 USA (kdobson@google.com)*

Abstract: Generating haptic forces in portable electronic devices and wearables is often accomplished with small vibrating motors, such as linear resonant actuators (LRAs). While these motors are favorably small, lightweight, inexpensive, and low-power, they are limited in the types of forces they can generate. Command-shaping techniques are presented that can either accentuate or attenuate haptic forces generated by LRAs. The proposed methods are advantageous because they generate force profiles that cannot be produced by standard haptic libraries. The methods are experimentally verified using a laser vibrometer.

Keywords: Haptics, Vibration, Command Shaping, Linear Resonant Actuator.

1. INTRODUCTION

Billions of smart phones, game controllers, touchscreens, keyboards, smart watches, and other devices contain small vibrating motors. These motors are used to provide haptic signals to users. Two classes of haptic motors are *eccentric rotating mass* (ERM) actuators and *linear resonant actuators* (LRAs). In both types of motors, haptic signals are generated when the motors vibrate and convey information to the user. While these motors offer many size, weight, cost, and efficiency advantages, their fundamental vibratory nature limits the types of forces they produce. This paper presents control methods that expand the haptic signal repertoire by both reducing and accentuating the natural vibratory response of haptic motors.

ERMs, like the ones shown in Figure 1, are comprised of a DC motor with an unbalanced mass attached to the motor shaft. When voltage is applied to the motor, the unbalanced mass rotates. This motion generates a radial force that rotates at the same frequency as the motor shaft. The oscillating force is perceived by users as "vibration."

The motor vibration from the ERM is what conveys the haptic signal to the user. The amplitude of the force is proportional to the square of the angular velocity of the shaft. Because the mass of the rotating imbalance is typically small, ERMs need to operate at a high angular velocity before haptic forces can be felt by the user. Many ERM-type motors are designed to operate at speeds that generate vibration in the 150-250 Hz range.

Motors that exhibit a rotating imbalance are more susceptible to certain types of failures than well-balanced motors. For instance, unbalanced motors must resist radial forces that would not be present on balanced motors. These forces are transmitted through shaft bearings or bushings, and can cause these elements to wear or fail prematurely.

LRAs, like the one shown in Figure 2, are structurally different from ERM actuators. They are essentially mass-spring systems that are contained within a housing. The motion of the mass is excited by forces generated by an electromagnet placed near the moving mass. The spring acts to return the displaced mass to its equilibrium position.

Fig. 1. ERM Motor [Precision Microdrives Ltd (2020a)]

[1] This research was done while the author was working for Pennington Advisors on assignment at Google LLC.

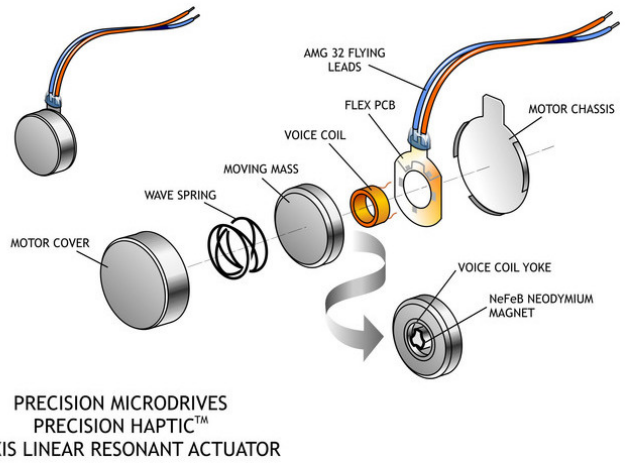

Fig. 2. LRA Motor [Precision Microdrives Ltd (2020b)]

LRAs are becoming more popular for haptic applications because they have several advantages over ERMs. Notably, they do not require unbalanced forces to be exerted on shaft bearings or bushings. Additionally, they also have more favorable haptic characteristics than ERMs because they can generate detectable forces over a larger range of frequencies, including lower frequencies. This dynamic characteristic exists because, unlike ERMs, where the magnitude of the forces are closely coupled with the driving frequency, the forces generated by LRAs are somewhat independent of the driving frequency. Furthermore, if LRAs are driven at the resonant frequency of the mass-spring system, then they can generate forces in a very efficient manner, which is especially important in applications with limited battery life.

The objectives of this paper are to explore the dynamics and improve the control of haptic motors in general, and LRAs in particular. To this end, the next section presents models that capture the primary dynamic aspects of LRAs. Section 3 then presents command-shaping methods that can be configured to either attenuate or accentuate the vibratory forces. Section 4 presents experimental measurements with a laser vibrometer that verify both the vibration reduction and the vibration accentuation of the command-shaping methods. Section 5 contains concluding remarks and summarizes key results.

2. LRA MODELING

The LRA schematic shown previously in Figure 2 can be modeled in the manner shown in Figure 3. This figure depicts an LRA housing of mass, m_1, and smaller, driven mass, m_2, typically made from a ferrous material. The driven mass is constrained to move within the housing along a horizontal axis. A spring couples the driven mass to the housing with spring constant k. Damping forces are represented by damping constant b. Driving forces imparted by an electromagnet are represented by F_d acting on the driven mass and housing in opposite directions. The displacements of the housing and driven mass from their at-rest positions are represented by x_1 and x_2, respectively.

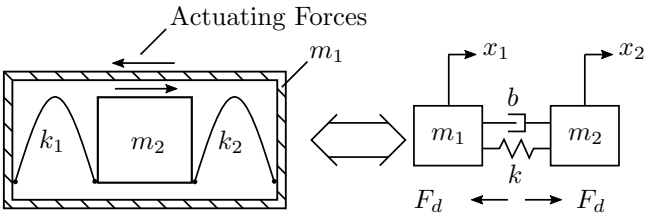

Fig. 3. Model of Linear Resonant Actuator.

2.1 Linear Dynamic Model

If both the spring and damper are linear in nature, then the reaction forces generated by these elements can be represented mathematically as:

$$\text{Spring Force} = k(x_1 - x_2) \tag{1}$$
$$\text{Damping Force} = b(\dot{x}_1 - \dot{x}_2) \tag{2}$$

State-Space Representation

The linear differential equations of motion for the LRA can be written in state-space form:

$$\dot{\mathbf{q}} = \begin{bmatrix} 0 & 1 & 0 & 0 \\ \frac{-k}{m_1} & \frac{-b}{m_1} & \frac{k}{m_1} & \frac{b}{m_1} \\ 0 & 0 & 0 & 1 \\ \frac{k}{m_2} & \frac{b}{m_2} & \frac{-k}{m_2} & \frac{-b}{m_2} \end{bmatrix} \mathbf{q} + \begin{bmatrix} 0 \\ \frac{-1}{m_1} \\ 0 \\ \frac{1}{m_2} \end{bmatrix} F_d \tag{3}$$

The state vector, $\mathbf{q}$ is defined as:

$$\mathbf{q} = [x_1 \ \dot{x_1} \ x_2 \ \dot{x_2}]^T \tag{4}$$

Transfer Function Representation

An alternative to the state-space equations of motion shown in (3) is to represent the relationship between the driving force and the displacement of the housing in the Laplace domain. Assuming zero initial conditions yields:

$$\frac{X_1(s)}{F_d(s)} = \frac{-1/m_1}{s^2 + s2\zeta\omega_n + \omega_n^2} \tag{5}$$

where

$$\omega_n^2 = k/m_{eq} \tag{6}$$
$$2\zeta\omega_n = b/m_{eq} \tag{7}$$
$$m_{eq} = (m_1 m_2)/(m_1 + m_2) \tag{8}$$

The linear behavior governed by the preceding equations of motion largely capture the actual behavior of some LRAs. This will be shown in a subsequent section. However, it will also be shown that some LRAs exhibit non-linear dynamics that are not captured well by a linear model. For these scenarios, a more general model is needed.

2.2 Nonlinear Dynamic Model

The unforced oscillation frequency of an LRA that exhibits predominantly linear dynamics will tend to remain constant, irrespective of spring elongation. Not all LRAs, however, exhibit this constancy. It has been observed in some

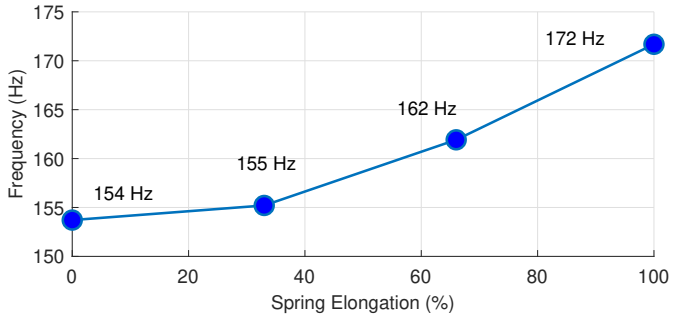

Fig. 4. Measured Oscillation Frequencies at Different Spring Elongation Positions.

LRAs that unforced oscillation frequency can increase with spring elongation. Experimental data for one such LRA is shown in Figure 4.

The behavior exhibited in this nonlinear LRA can be modeled by generalizing Hooke's law:

$$\text{Spring Force} = k(x_1 - x_2) \tag{9}$$

where the spring coefficient is obtained from a function κ:

$$k = \kappa(\text{elongation}) \tag{10}$$

Since oscillation frequency increases with spring stiffness, a κ function that models the behavior exhibited in Figure 4 should increase the spring constant with spring elongation. One such function is:

$$k = k_o(1 + \rho|d|^{\lambda}) \tag{11}$$

where d is the spring elongation, defined as:

$$d \equiv x_1 - x_2 \tag{12}$$

The symbols, k_o, ρ, and λ are adjustable parameters that can be used to tune the behavior of the model. More specifically, k_o is the minimum spring stiffness output from the function in the absence of any spring deflection. ρ and λ are positive scalars that increase the spring stiffness when $d > 0$.

In light of (11), it may be shown that the dynamics of the nonlinear LRA model may be expressed as:

$$\ddot{d} + 2\zeta\widetilde{\omega}_n\dot{d} + \widetilde{\omega}_n^2 d = \frac{-F_d(t)}{m_{eq}} + \frac{k_o}{m_{eq}}\rho\lambda\bar{d}^{(\lambda+1)} \tag{13}$$

where

$$\widetilde{\omega}_n^2 \equiv \frac{k_o}{m_{eq}}\left(1 + \rho(\lambda+1)\bar{d}^{\lambda}\right) \tag{14}$$

$$2\zeta\widetilde{\omega}_n \equiv \left(\frac{\beta}{m_{eq}}\right) \tag{15}$$

The symbol $\bar{d}$ represents the steady-state elongation corresponding with a steady state force, $\bar{F}_d$.

Equation (14) is significant. It reveals the relationship between the natural frequency, $\widetilde{\omega}_n$, of the system when it oscillates about the equilibrium point $\bar{d}$. This frequency changes with $\bar{d}$, and can be precisely adjusted using the parameters k_o, λ, and ρ.

3. COMMAND-SHAPING METHODS

Given that LRAs are mass-spring systems that naturally vibrate in response to an input, they can exhibit unwanted vibration, or "buzzing," that is uncomfortable or annoying. Therefore, it would be useful in certain applications to drive the motors without generating high levels of "buzz." One way to decrease residual vibration is to use input shaping, which is a command-filtering method that limits unwanted vibration [Smith (1958); Singer and Seering (1990); Singhose (2009); Singh and Vadali (1994); Singh (2009); Vyhlidal and Hromik (2015)]. Input shaping has been used on a great variety of systems ranging from large cranes [Sorensen et al. (2007)] down to very small systems [Fortgang et al. (2004)].

Figure 5 shows the fundamental input-shaping concept. In the top of Figure 5, a first impulse is applied to a flexible linear system, and induces a lightly-damped response. A similar response (shown by the dashed line) would result if a second impulse were applied a short time later. The bottom of Figure 5 shows the response that results from both impulses. If the system is linear and time-invariant, then the two responses combine linearly and the vibration is eliminated.

In order to implement input shaping on real systems, a vibration-reducing impulse sequence, like that shown in Figure 5, is convolved with a baseline command to create a shaped command that preserves the vibration-reducing properties of the impulse sequence. An example of a shaped step input is shown in Figure 6. In the top plot, the Step 1 command is applied to a flexible linear system, and the system vibrates in response. A similar result would occur should the Step 2 command be issued a short time later. The bottom of Figure 6 shows the response that would result if the command was the sum of Steps 1 and 2.

Input-shaped step sequences may consist of more than two steps. The amplitudes and times of the steps may be written in matrix form as:

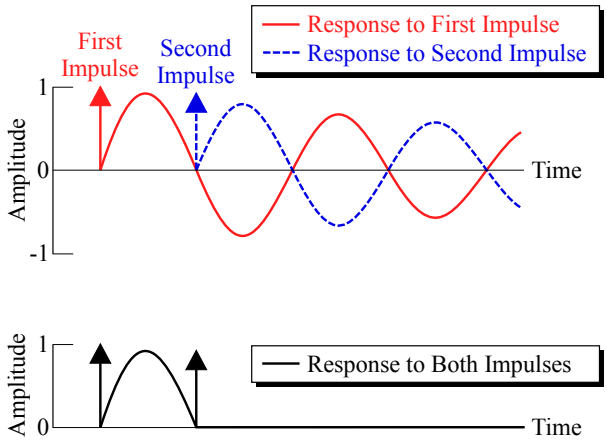

Fig. 5. Response of a Linear System to a Sequence of Impulses.

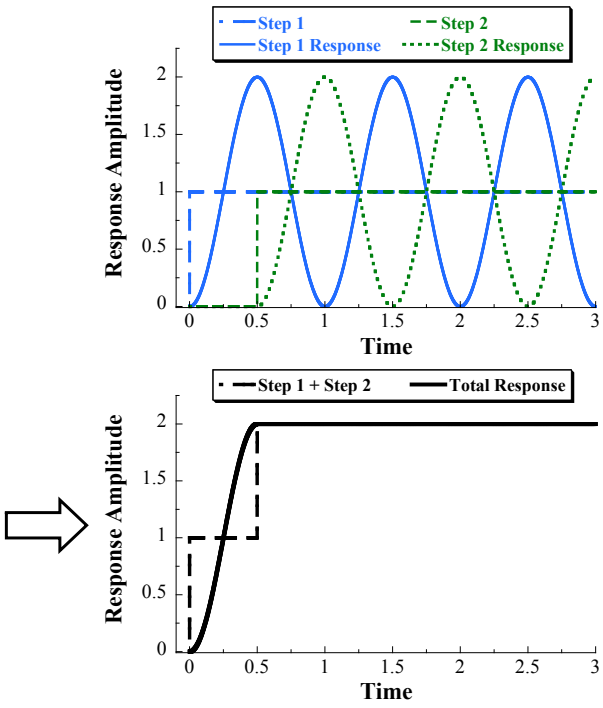

Fig. 6. Creating an Input-Shaped Step Sequence by Combining Two Step Commands.

$$\begin{bmatrix} A_i \\ t_i \end{bmatrix} = \begin{bmatrix} A_1 & \dots & A_i & \dots & A_N \\ t_1 & \dots & t_i & \dots & t_N \end{bmatrix} \tag{16}$$

where A_i are the step amplitudes, t_i are the time locations of each step, and N is the number of impulses.

The step amplitudes and time locations are designed using estimated natural frequencies and damping ratios of the flexible modes to be suppressed. Input shapers can be made robust to errors and changes in these parameters [Singer and Seering (1990); Singhose et al. (1994, 1996)].

3.1 Design Constraints and Performance Requirements

Input shapers may be designed using different combinations of performance requirements. For example, one set of constraints consists of requiring zero residual vibration at the time of the last step and restricting the steps to be positive. The residual vibration resulting from a sequence of impulses applied to an underdamped system can be calculated using [Singer and Seering (1990)]:

$$V(\omega_n, \zeta) = e^{-\zeta \omega_n t_n} \sqrt{[C(\omega_n, \zeta)]^2 + [S(\omega_n, \zeta)]^2} \tag{17}$$

where

$$C(\omega_n, \zeta,) = \sum_{i=1}^{n} A_i e^{\zeta \omega_n t_i} cos(\omega_d t_i) \tag{18}$$

and

$$S(\omega_n, \zeta,) = \sum_{i=1}^{n} A_i e^{\zeta \omega_n t_i} sin(\omega_d t_i) \tag{19}$$

The symbols ω_n and ζ are the natural frequency and damping ratio of the flexible mode. A_i and t_i are the amplitudes and time locations of the impulses, n is the number of impulses in the impulse sequence, t_n is the time location of the final impulse, and the damped natural frequency is:

$$\omega_d = \omega_n \sqrt{1 - \zeta^2} \tag{20}$$

When V is set to zero, (17) results in a zero residual vibration constraint.

Due to the transcendental nature of (17), there are multiple solutions that yield zero residual vibration. To make the solution time optimal subject to the zero residual vibration and amplitude constraints, the input shaper duration must be as short as possible. The time optimality constraint is:

$$\min(t_n). \tag{21}$$

For an undamped flexible mode, a *Zero Vibration* (ZV) [Smith (1958)] input-shaped step sequence has amplitudes and times:

$$\begin{bmatrix} A_i \\ t_i \end{bmatrix} = \begin{bmatrix} 0.5 & 0.5 \\ 0 & \frac{T_n}{2} \end{bmatrix} \tag{22}$$

where T_n is the vibration or oscillation period. This is the sequence of steps used in Figure 6 to create a command that results in zero residual vibration for a flexible system with a period of $T_n = 1$.

The above shaper is designed using the requirement that the impulse amplitudes be positive. If that requirement is relaxed to allows negative amplitudes, then the shaper can act more quickly to suppress residual vibration. If the amplitudes are allowed to range between positive 1 and negative 1, then such a *Unity-Magnitude Zero-Vibration* (UMZV) shaper for undamped systems can be described as:

$$\begin{bmatrix} A_i \\ t_i \end{bmatrix} = \begin{bmatrix} 1 & -1 & 1 \\ 0 & \frac{cos^{-1}(0.5)}{\omega} & \frac{cos^{-1}(-0.5)}{\omega} \end{bmatrix} \tag{23}$$

Formulas that give the UMZV shaper for damped systems are available in the literature [Singhose (2009)].

4. EXPERIMENTAL TESTING OF SHAPING METHODS

4.1 Measurement System

Measurements of LRA motion were conducted with a Laser Doppler Vibrometer. A vibrometer measures the frequency difference between an internal reference beam and a second beam directed at the surface of the test substrate. Reflective tape was mounted on the surface of coin-shaped LRAs. The motors themselves were mounted on a sheet of neoprene foam with a pressure sensitive adhesive to allow for motion in both the up and down directions. A schematic diagram of the experimental setup is shown in Figure 7(a).

The Polytec Laser Vibrometer used for the tests reported here can measure velocity and displacement of the test surface at a frequency of 250 kHz. Figure 7(b) shows a photograph of the the experimental setup with the laser vibrometer measuring an actuator mounted on neoprene foam. Figure 7(c) shows a close-up view of the motor and a diagram explaining the layers.

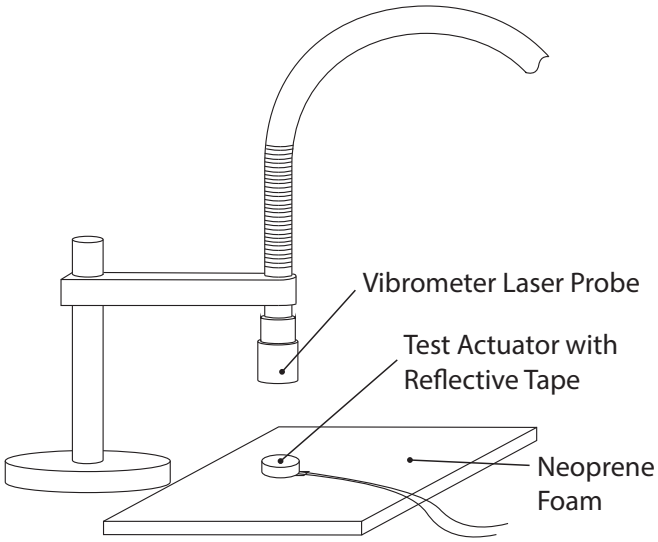

(a) Schematic Diagram.

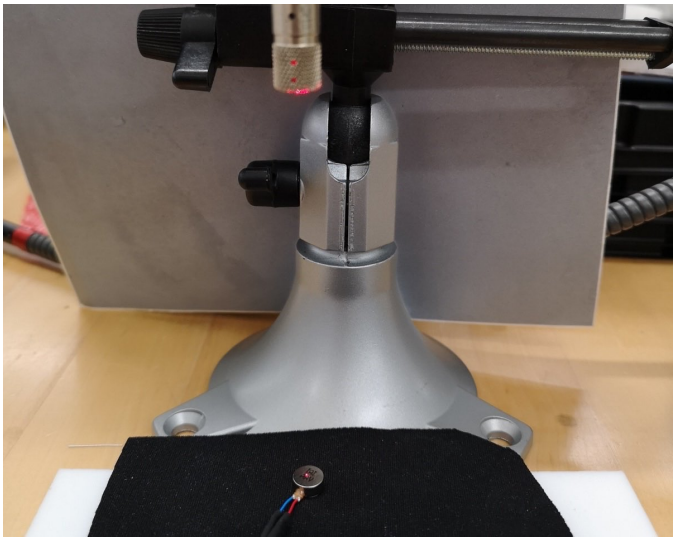

(b) Photograph of Experimental Setup.

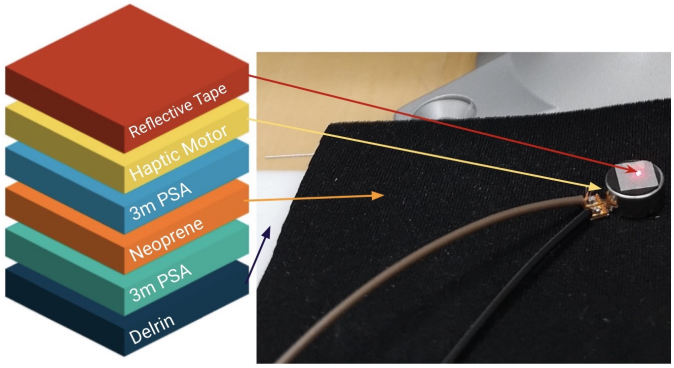

(c) Close-up Photograph of Motor Mount and Layer Diagram.

Fig. 7. Laser Vibrometer Setup and Photos.

Experiments were conducted on a variety of LRAs. The largest LRA used was the G1040003D LRA (Jinlong Machinery & Electronics, Inc.) This LRA is a coin-shaped actuator with a diameter of 10mm and a height of 4.05 mm. The actuator is rated for a maximum voltage of 2.5 Vrms and is rated to vibrate at a resonant frequency of 170 ± 5 Hz. The LRA is rated to produce a minimum acceleration of 1.8 Grms at its resonant frequency. [2] The LRA was controlled using an Arduino Uno board with an attached motor driver shield (Pololu DRV8835 Dual Motor Driver Shield for Arduino.) The smallest LRA used was the G0832022D (Jinlong Machinery & Electronics, Inc.) This smaller LRA is a coin-shaped actuator with a diameter of 8 mm and a height of 3.2 mm. The actuator is rated for a maximum voltage of 2.0 Vrms and is rated to vibrate at a resonant frequency of 235 Hz.

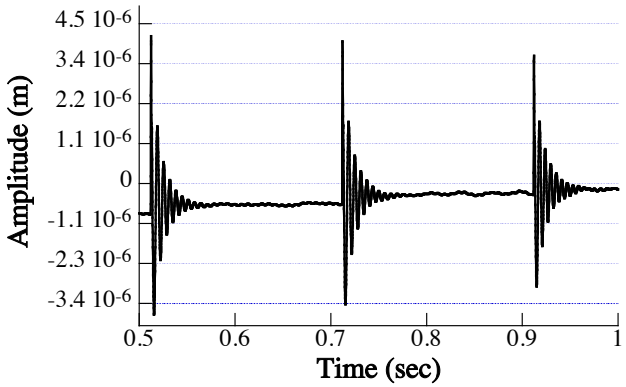

Fig. 8. Step Responses to Three Incremental Increases in Voltage.

4.2 Step and Sine Wave Responses

The open-loop step response of the large LRA was measured by applying three input steps: 0 to 1, 1 to 2, and 2 to 3 volts. The measurements of the motor responses to these three steps are shown in Figure 8. The responses show that the amplitude of each 1 volt step decreases slightly as the voltage is increased. Additionally, though not readily visible in the plot of Figure 8, the frequency of the response increases slightly with voltage. The average frequency and damping ratio from these responses was used to select the modeling parameters for this motor.

The open-loop response of the small LRA was measured by applying sine waves of various durations. More specifically, four sinusoidal voltage intervals were issued, each with a frequency of 210 Hz. The four interval durations were 1 cycle, 1.25 cycles, 1.5 cycles, and 1.75 cycles. The measurements of the motor responses to these four inputs are compared to the simulated responses in Figure 9. The responses show that the amplitude of response increases as the duration of the sine wave input increases. The results also show that the model is able to accurately predict the response of the actual motor.

4.3 Measurements of Internal Mass Motion

The preceding tests measured the surface of the LRA housing. In order to better understand the dynamics of the internal LRA structure, the top section of the motor casing was removed. The remaining structure consisted of the base plate with the coil, the spring, and the vibrating mass. Step voltage commands were issued to the coil while

[2] www.vibration-motor.com/wp-content/uploads/2019/05/G1040003D.pdf.

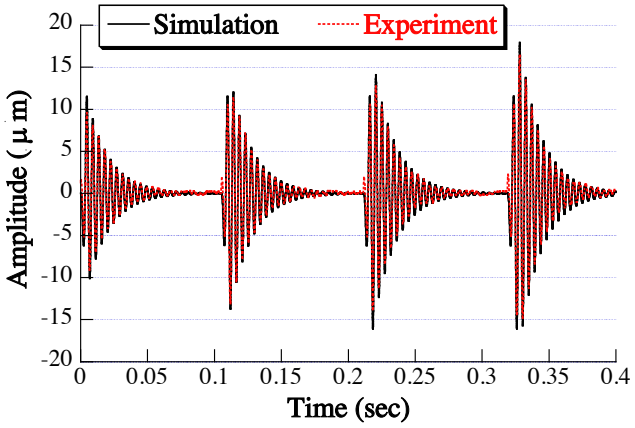

Fig. 9. Simulated and Measured Responses to Sine Waves of Various Durations.

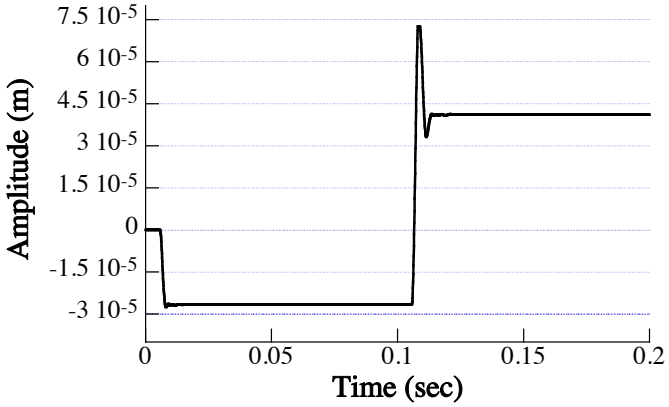

Fig. 10. Measured Step Responses of Internal Mass.

the laser vibrometer was used to record the motion of the mass.

The responses to both full negative and full positive voltage steps are shown in Figure 10. A negative displacement response indicates that the mass is stretching the spring and moving away from the coil. A positive displacement response indicates that the mass is compressing the spring and moving closer to the coil.

The responses reveal a nonlinear effect, wherein voltages that pull the mass closer to the coil create a larger displacement than voltages that push the mass away from the coil. For the same voltage, the motor mass moves approximately 50% further when pulled toward the coil. Such nonlinear effects are to be expected given the nonlinear magnetic field generated by the energized coil. However, some portion of the nonlinear effect can be attributed to nonlinear spring effects. In any case, the results indicate that linear input-shaping methods will not work perfectly, but they may still work well. The next section examines the application of linear input-shaping methods to LRAs.

4.4 Vibration-Reducing Commands

Both the step commands and the sine commands described above induced significant residual vibration of the LRA motors. Such responses are useful when the desired effect of the user is a "buzz." However, in order to achieve a

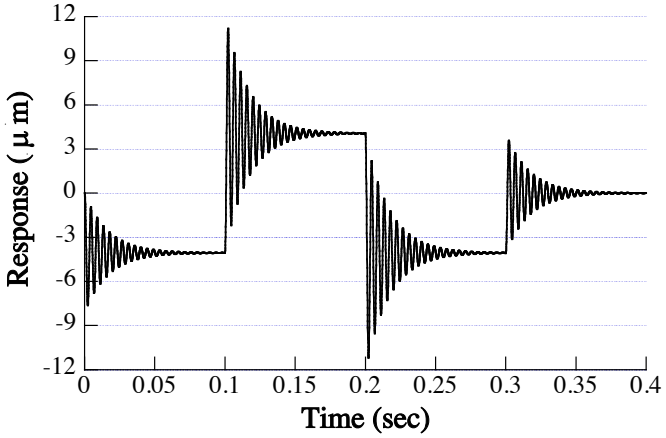

a) Simulated Response to Unshaped Steps.

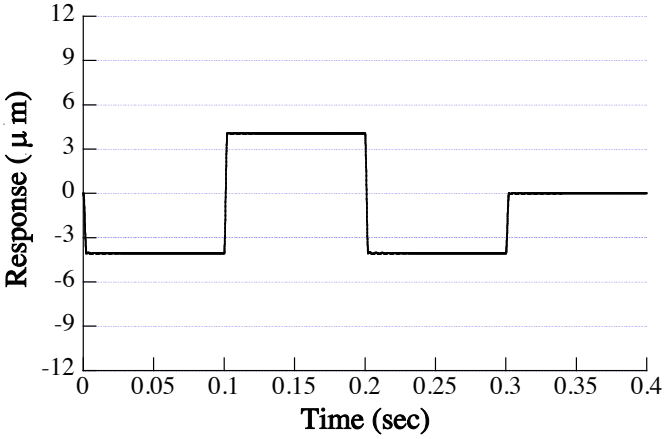

b) Simulated Response to ZV-Shaped Steps.

Fig. 11. Simulated ZV-Shaped Step Responses of the G0832022D.

clear and crisp haptic force, it is useful to drive the motors without large amounts of residual vibration. Such driving commands can be designed using the input-shaping methods described above. Figure 11a) shows the simulated response of the small LRA motor to a series of three pulses - negative, positive, negative. Note that such a sequence of three pulses is composed of 4 step inputs: 0 to -1, -1 to 1, 1 to -1, and -1 back to 0. Figure 11b) shows the simulated response when a ZV input shaper is used to modify the sequence of four steps. The ZV input shaper virtually eliminates the "buzzing" from the simulated LRA motor.

The preceding sequence of unshaped and ZV-shaped steps were implemented on the actual LRA. Again the vibrometer was used to measure the response to the commands. The ZV commands were designed for the small LRA using experimentally-determined vibration parameters of 224.6 Hz and a damping ratio of 0.042. Figure 12(a) shows the response to the unshaped steps and Figure 12(b) shows the response to the ZV-shaped steps. The figure demonstrate that significant attenuation of the "buzzing" - approximately 50% - was achieved using the ZV-shaped commands.

The preceding demonstrated that the "buzz" exhibited by an LRA can be reduced with input shaping. However, as demonstrated in Figure 12b), reducing the buzz was

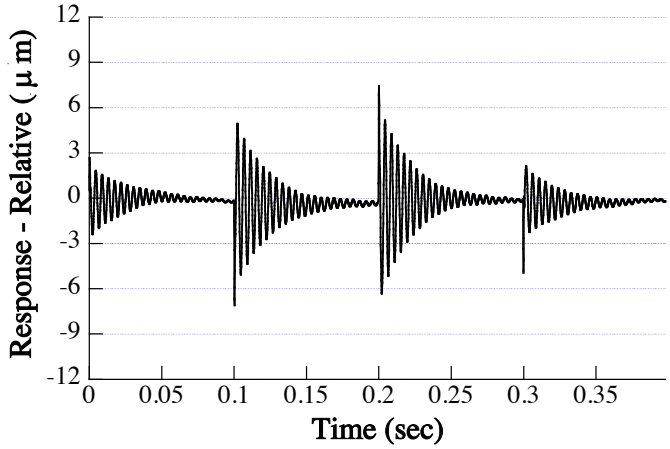

(a) Experimental Response to Unshaped Steps.

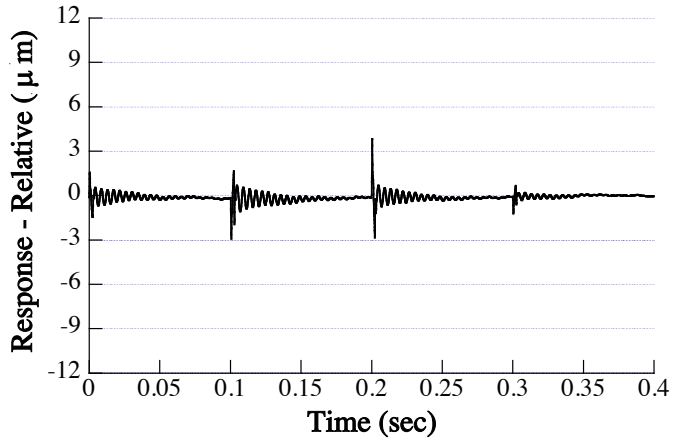

(b) Experimental Response to ZV-Shaped Steps.

Fig. 12. Experimentally-Measured ZV-Shaped Step Responses of the G0832022D.

achieved at the expense of reducing the peak acceleration exhibited by the LRA. Consequently, a user would also experience a reduction in the felt haptic force. Stated differently, the shaped response provides a weaker haptic signal.

In order to achieve a larger haptic signal, while still achieving a reduction in buzzing, a UMZV shaper was implemented. This type of shaper uses the same maximum acceleration as the unshaped step inputs, therefore, it provides a large haptic signal. Figure 13 shows the response to the UMZV shaper. This shaper is somewhat more sensitive to modeling errors and the nonlinear behavior of the LRA, so it produces somewhat more residual buzz than was caused by the ZV shaper. However, the UMZV provides a very useful haptic effect because it provides a strong response, with significantly less buzz than the unshaped step input.

4.5 Vibration-Accentuating Commands

Usually, command-shaping methods are used to attenuate vibration. However, input shaping can also be used to amplify vibration. Such an approach has been used previously to accentuate the swing of a wrecking ball [Maleki et al. (2014)]. For haptic force generation, this approach allows a given linear resonant actuator to produce a stronger haptic effect for the same maximum rated voltage.

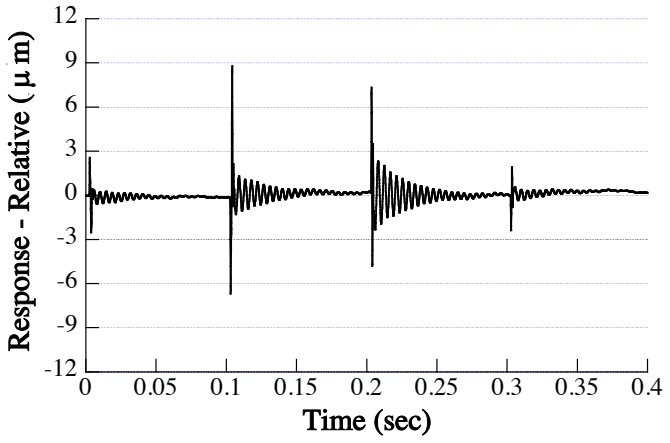

Fig. 13. Experimentally-Measured UMZV-Shaped Step Responses of the G0832022D.

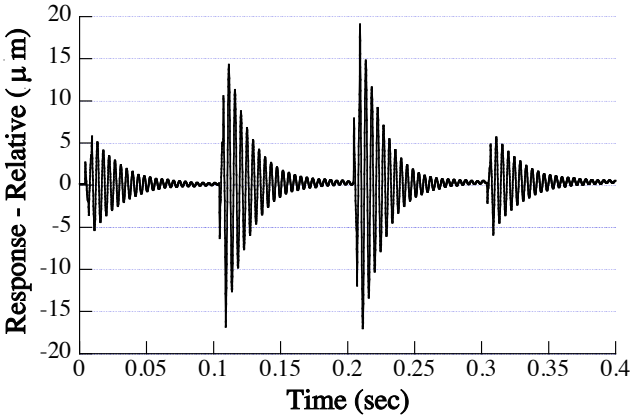

Fig. 14. Vibration-Accentuated Step Responses of the G0832022D.

The vibration-accentuating shaper implemented for this study was a UMZV shaper that was intentionally designed to amplify, instead of attenuate, vibration. Instead of using the actual natural frequency of the LRA when designing the shaper, a value of 1/3 of the natural frequency was used. This has the effect of causing each impulse in the shaper to reinforce the vibration caused by the previous impulse in the sequence. Figure 14 shows the experimental response of the small LRA to this vibration-accentuating shaped command signal. Note that the range of the vertical response axis has been increased from 12 to 20 to show the full extent of the motion. This shaped signal was very effective at exciting the motor and produced a very large haptic effect.

5. CONCLUSIONS

The range and diversity of appreciable forces generated by small haptic motors can be greatly extended by shaping the command signals used to drive the motors. A dynamic model of LRA motors was developed and used to predict the behavior in response to various types of command signals. Command-shaping methods were used to drive the motors such that the inherent "buzzing" of the LRA was significantly reduced, while preserving the

amplitude of the haptic force felt by the user. Additionally, the command-shaping method was altered to achieve the opposite extreme of accentuating the LRA vibration such that the haptic forces are very large. Experimental testing with a laser vibrometer confirmed both the reduction and accentuation of the LRA vibration.

REFERENCES

Fortgang, J., Marquez, J.d.J., and Singhose, W. (2004). Application of input shaping on micro-mills. In *Japan – USA Symposium on Flexible Automation*. Denver, Colorado.

Maleki, E., Singhose, W., and Gurleyuk, S.S. (2014). Increasing crane payload swing by shaping human operator commands. *IEEE Transactions on Human-Machine Systems*, 44(1), 106–114.

Precision Microdrives Ltd (2020a). 306-006 PCB Vibration Motor. `https://www.precisionmicrodrives.com/wp-content/uploads/2018/05/306-006-pcb-vibration-motor.original.png`. Accessed: 2020-03-16.

Precision Microdrives Ltd (2020b). Precision Microdrives Y-axis LRA Linear Vibrator Motor. `https://www.precisionmicrodrives.com/wp-content/uploads/2018/05/lra-linear-vibrator-construction.original.jpg`. Accessed: 2020-03-16.

Singer, N.C. and Seering, W.P. (1990). Preshaping command inputs to reduce system vibration. *Journal of Dynamic Systems, Measurement, and Control*, 112, pp. 76–82.

Singh, T. (2009). *Optimal Reference Shaping for Dynamical Systems: Theory and Applications*. 978-1439805626. CRC Press.

Singh, T. and Vadali, S.R. (1994). Robust time-optimal control: A frequency domain approach. *J. of Guidance, Control and Dynamics*, 17, 346–353.

Singhose, W. (2009). Command shaping for flexible systems: A review of the first 50 years. *Int. J. of Precision Engineering and Manufacturing*, 10(4), 153–168.

Singhose, W., Seering, W., and Singer, N. (1994). Residual vibration reduction using vector diagrams to generate shaped inputs. *ASME J. of Mechanical Design*, 116(June), 654–659.

Singhose, W., Seering, W., and Singer, N. (1996). Input shaping for vibration reduction with specified insensitivity to modeling errors. In *Japan-USA Sym. on Flexible Automation*, volume 1, 307–13. Boston, MA.

Smith, O. (1958). *Feedback Control Systems*. McGraw-Hill Book Co., Inc., New York.

Sorensen, K., Singhose, W., and Dickerson, S. (2007). A controller enabling precise positioning and sway reduction in bridge and gantry cranes. *Control Engineering Practice*, 15(7), 825–837.

Vyhlidal, T. and Hromik, M. (2015). Parameterization of input shapers with delays of various distribution. *Automatica*, 59, 256–263.